

## ORIGINAL RESEARCH

# Impact of stator interturn short circuit fault on shaft voltage in a synchronous generator

Yu-Ling He<sup>1</sup>  | Pei-Jie Yang<sup>1</sup> | Kai Sun<sup>1</sup> | Zhen-Li Xu<sup>1</sup> | Hai-Peng Wang<sup>1</sup>  | Xian-Long He<sup>2</sup> | David Gerada<sup>3</sup>

<sup>1</sup>Department of Mechanical Engineering, North China Electric Power University, Baoding, Hebei, China

<sup>2</sup>Hebei Zhenchuang Electronic Technology Co., LTD, Langfang Yanjiao Development Zone, Baoding, China

<sup>3</sup>Department of Electrical and Electronics Engineering, University of Nottingham, University Park, Nottingham, UK

## Correspondence

Hai-Peng Wang, Hebei Key Laboratory of Electric Machinery Health Maintenance and Failure Prevention, North China Electric Power University, Baoding 071003, China.  
Email: 52452403@ncepu.edu.cn

## Funding information

Natural Science Foundation of Hebei Province, Grant/Award Number: E2020502031; Chinese Fundamental Research Funds for the Central Universities, Grant/Award Numbers: 2020MS114, and 2018YQ03; 3rd Top Youth Talent Support Program of Hebei Province, Grant/Award Number: [2018]-27; National Natural Science Foundation of China, Grant/Award Number: 52177042; Suzhou Social Developing Innovation Project of Science and Technology, Grant/Award Number: SS202134

## Abstract

Shaft voltage often exists in synchronous generators due to the assembly error or various faults after the long-term performance. The article investigates the shaft voltage characteristic under the stator interturn short circuit (SISC) condition. Different from other studies, this article mainly considers the mapping relationship between the amplitude–frequency characteristics of the shaft voltage and the SISC degrees. The detailed shaft voltage expressions are first derived based on the magnetic flux density under the normal condition and SISC condition. Then the finite element analysis and the experiment is studied on a CS-5 prototype synchronous generator with two poles in order to validate the theoretical formula. The result shows that there is no shaft voltage in the normal condition, while the shaft voltage is generated obviously under the SISC condition. Meanwhile, the frequency component of the shaft voltage is mainly composed of odd harmonics including the first, third and fifth harmonics.

## KEYWORDS

asymmetrical magnetic flux density, shaft voltage, stator interturn short circuit, synchronous generator

## 1 | INTRODUCTION

Synchronous generators play an irreplaceable role in the electrical power system. Safe and the stable operation is extremely important for the synchronous generator. The shaft voltage is induced in the shaft of the synchronous generator due to the asymmetry load distribution, the rotor eccentricity, the rotor/stator interturn short circuit etc. The shaft voltage reduces the mechanical strength of the shaft and damages the bearings [1–3]. Therefore, it is significant to comprehensively study the inherent characteristics of the shaft voltage under the typical running conditions in order to fully monitor and control the shaft voltage.

Many studies on the presence of the shaft voltage have been reported since the last century [4]. For instance, Alger obtained the causes of the shaft voltage using theoretical calculation and experimental verification [5]. Hereafter, more scholars perfected the theoretical mechanism of the shaft voltage, which can be summarised as follows [1, 6–8]:

- (a) Unbalanced magnetic fields caused by design, manufacturing, and rotor eccentricity.
- (b) Turbonator with a static excitation system.
- (c) Electrostatic effect.
- (d) Axial rotor flux.

**Abbreviations:** EMF, electromotive force; FEA, finite element analysis; MFD, magnetic flux density; MFL, magnetic flux lines; MMF, magnetomotive force; PPUA, permeance per unit area; SAGE, static air-gap eccentricity; SISC, stator interturn short circuit.

This is an open access article under the terms of the Creative Commons Attribution-NonCommercial-NoDerivs License, which permits use and distribution in any medium, provided the original work is properly cited, the use is non-commercial and no modifications or adaptations are made.

© 2022 The Authors. *IET Electric Power Applications* published by John Wiley & Sons Ltd on behalf of The Institution of Engineering and Technology.

Further, according to the mechanism of the shaft voltage, many effective measures are carried to reduce the shaft voltage. Peng selected the appropriate pole-arc coefficient to weaken the shaft voltage in the permanent magnet generator [9]. Meanwhile, Chen summarised the research status and the prevention measures of the shaft voltage [10]. Generally, the weakening and the prevention of the shaft voltage can be summarised as follows [11, 12]:

- (a) Grounding of the gas measuring shaft.
- (b) Bearing pedestal insulation.
- (c) Carbon brush is installed on the shaft.

Different kinds of electrical and mechanical faults occur in synchronous generators after long-term operation [13]. Comparing with the normal condition, the shaft voltage obviously increases due to the asymmetric magnetic field under the fault and presents the clear time–frequency characteristic. Hence, the shaft voltage is utilised to the fault diagnosis in the generators [14].

By far, the shaft voltage is comprehensively analysed under mainly the rotor interturn short circuit and the static air-gap eccentricity. For instance, Wu et al. conducted a series of studies on the shaft voltage in detail. The distorted magnetic field is analysed using the air-gap conductance method under the typical rotor fault, and the shaft voltage signal is obtained to detect the typical rotor fault [15]. Meanwhile, the characteristic frequency of the shaft voltage signal and the number of the stator slots are closely related due to the cogging effect, which provides the criteria for the diagnosis of the rotor interturn short circuit [16]. Besides, Darques explored the impact of the end windings on the shaft voltage using finite element analysis (FEA) [17].

Stator interturn short circuit (SISC) is a common fault due to the insulation damage caused by the mechanical vibration and the excessive temperature in synchronous generators [18, 19]. Bouzid observed the changes of the three-phase current and voltage to monitor the SISC fault in motors [20]. Sarikhani used the electromotive force (EMF) to judge the SISC fault [21]. The above research mainly focusses on the characteristics of the electromechanical parameters under SISC fault, while the common shaft voltage is ignored in synchronous generators.

In this work, we comprehensively analyse the characteristics of the shaft voltage under the SISC fault using the theoretical analysis. And the FEA calculation and the experiment are carried out. The contribution of this paper mainly includes three aspects: (1) the detailed shaft voltage expression under the SISC fault is derived, (2) the simulation model of the shaft voltage in synchronous generators is established by the rotating shaft equivalent substitution, and (3) a specific device to test the shaft voltage is designed and manufactured by the authors.

The remainder of the paper is organised as follows: In Section 2, the theoretical model of the shaft voltage is proposed under the SISC fault in detail, while the FEA and the experimental tests are carried out in Section 3. Finally, the primary conclusions of the paper are drawn up in Section 4.

## 2 | THEORETICAL MODEL

The magnetic flux density (MFD) is the basic parameter for calculating the shaft voltage of the generator. The MFD can be obtained by multiplying the magnetomotive force (MMF) and the permeance per unit area (PPUA) [22].

### 2.1 | MFD model

The air-gap magnetic field is symmetrically distributed under the normal condition, and PPUA and MMF can be respectively written as follows [23]:

$$\Lambda = \frac{\mu_0}{g_0} = \Lambda_0 \quad (1)$$

$$\begin{aligned} f(\alpha_m, t) = & F_s \cos(\omega t - p\alpha_m) \\ & + F_r \cos\left(\omega t - p\alpha_m + \varphi + \frac{\pi}{2}\right) \end{aligned} \quad (2)$$

where  $g_0$  is the average length of radial air-gap,  $F_s$  and  $F_r$  are the stator MMF and the rotor MMF, respectively,  $\alpha_m$  is the mechanical angle used to indicate the circumferential position of the air-gap,  $\varphi$  is the internal power angle of the generator, and  $p$  is the number of pole pairs.

Further, MFD can be written as follows:

$$\begin{aligned} B_1(\alpha_m, t) = & f_d(\alpha_m, t)\Lambda_0 \\ = & [F_s \cos(\omega t - p\alpha_m) \\ & + F_r \cos\left(\omega t - p\alpha_m + \varphi + \frac{\pi}{2}\right)]\Lambda_0 \end{aligned} \quad (3)$$

However, as SISC takes place, an additional circulating current ( $I_d$ ) will be induced in the short-circuit ring, as shown in Figure 1. The circulating current produces the pulsating magnetic field, which centres on the short-circuit winding axis. The frequency of the new magnetic field is in agreement with the short-circuit current and can be expressed as follows:

$$\begin{aligned} f_d(\alpha_m, t) = & F_d \cos \omega t \cos(\alpha_m - \alpha_m') \\ = & F_{d+} \cos[\omega t - (\alpha_m - \alpha_m')] \\ & + F_{d-} \cos[\omega t + (\alpha_m - \alpha_m')] \end{aligned} \quad (4)$$

where  $F_{d+}$  and  $F_{d-}$  are the forwardly and the inversely rotating MMF amplitude, respectively, and  $\alpha_m'$  is the angle of the central position of the short-circuit turns.

Normally, the MMF forwardly rotates at the synchronous speed as the rotor. There is no extra electromotive force in the excitation windings. However, the inversely rotating MMF induces an extra electromotive force at  $2\omega$  due to the rotating

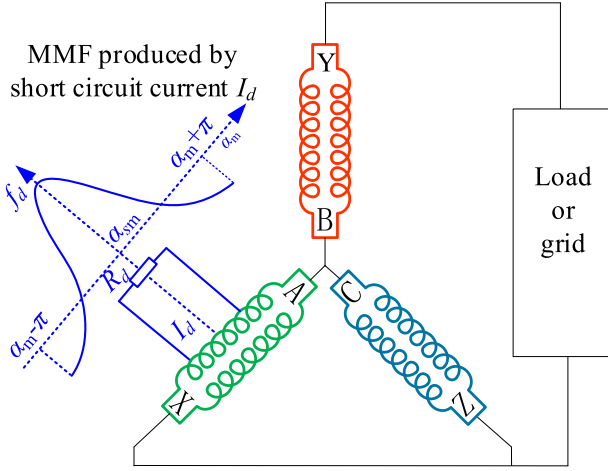


FIGURE 1 Diagrams of the stator interturn short circuit (SISC) fault.

direction difference between the rotor and the inversed MMF under the SISC condition. Hence, the excitation current in the field windings under the SISC condition can be expressed as follows:

$$\begin{aligned} I_f(\alpha_m, t) &= I_{f0} - I_{f2} \cos 2\omega t \cos \alpha_m \\ &= I_{f0} - \frac{1}{2}I_{f2} \cos(2\omega t + \alpha_m) \\ &\quad - \frac{1}{2}I_{f2} \cos(2\omega t - \alpha_m) \end{aligned} \quad (5)$$

where  $I_{f0}$  is the DC component in the field windings produced by the exciting system, while  $I_{f2}$  is the current induced under the SISC condition.

Further,  $F_r$  caused by the excitation current under the SISC fault can be written as follows:

$$\begin{aligned} F(\alpha_m, t) &= I_f(\alpha_m, t)N \\ &= I_{f0}N - \frac{1}{2}I_{f2} \cos(2\omega t + \alpha_m)N \\ &\quad - \frac{1}{2}I_{f2} \cos(2\omega t - \alpha_m)N \end{aligned} \quad (6)$$

where  $N$  is the turn number of each pole.

The EMFs of the three phases can be written as follows:

$$\left\{ \begin{aligned} e_a(t) &= F(\alpha_m, t)\Lambda_0 K \cos \omega t \\ &= I_{f0}KN\Lambda_0 \cos \omega t - \frac{1}{4}I_{f2}KN\Lambda_0 \cos(\omega t + \alpha_m) \\ &\quad - \frac{1}{4}I_{f2}KN\Lambda_0 \cos(3\omega t + \alpha_m) - \frac{1}{4}I_{f2}KN\Lambda_0 \cos(\omega t - \alpha_m) \\ &\quad - \frac{1}{4}I_{f2}KN\Lambda_0 \cos(3\omega t - \alpha_m) \\ e_b(t) &= F(\alpha_m, t)\Lambda_0 K \cos(\omega t - 120^\circ) \\ &= I_{f0}KN\Lambda_0 \cos(\omega t - 120^\circ) - \frac{1}{4}I_{f2}KN\Lambda_0 \cos(\omega t + \alpha_m + 120^\circ) \\ &\quad - \frac{1}{4}I_{f2}KN\Lambda_0 \cos(3\omega t + \alpha_m - 120^\circ) - \frac{1}{4}I_{f2}KN\Lambda_0 \cos(\omega t - \alpha_m + 120^\circ) \\ &\quad - \frac{1}{4}I_{f2}KN\Lambda_0 \cos(3\omega t - \alpha_m - 120^\circ) \\ e_c(t) &= F(\alpha_m, t)\Lambda_0 K \cos(\omega t + 120^\circ) \\ &= I_{f0}KN\Lambda_0 \cos(\omega t + 120^\circ) - \frac{1}{4}I_{f2}KN\Lambda_0 \cos(\omega t + \alpha_m - 120^\circ) \\ &\quad - \frac{1}{4}I_{f2}KN\Lambda_0 \cos(3\omega t + \alpha_m + 120^\circ) - \frac{1}{4}I_{f2}KN\Lambda_0 \cos(\omega t - \alpha_m - 120^\circ) \\ &\quad - \frac{1}{4}I_{f2}KN\Lambda_0 \cos(3\omega t - \alpha_m + 120^\circ) \end{aligned} \right. \quad (7)$$

where  $K = 2q\omega_c k_{w1} \tau f L$ ,  $q$  is the slot number for each phase per pole,  $\omega_c$  is the turn number of each coil,  $k_{w1}$  is the fundamental winding factor,  $\tau$  is the polar distance,  $f$  is the fundamental frequency, and  $L$  is the length of the stator core.

As indicated in (7), the induced EMF for each phase is composed of five parts. Based on the phase angles of the three phases, the first part forms the MMF rotating in the forward direction at the fundamental frequency speed, while the second and fourth parts form a backwardly rotating MMF at the fundamental frequency. Meanwhile, the third and fifth parts form the forwardly rotating MMFs at  $3\omega$ . Consequently, the MFD expression based on (3), (6) and (7) under the normal and SISC conditions can be written as follows:

$$\left\{ \begin{array}{l} B_1(\alpha_m, t) = \left[ F_r \cos\left(\omega t - p\alpha_m + \varphi + \frac{\pi}{2}\right) + F_s \cos(\omega t - p\alpha_m) \right] \Lambda_0 \\ \quad = \left[ I_{f0} N \cos\left(\omega t - p\alpha_m + \varphi + \frac{\pi}{2}\right) \right. \\ \quad \quad \left. + \eta I_{f0} N \cos(\omega t - p\alpha_m) \right] \Lambda_0 \quad \dots \dots \text{Normal} \\ B_2(\alpha_m, t) = I_{f0} N \Lambda_0 \cos(\omega t - \alpha_m + 0.5\pi + \varphi) \\ \quad - \frac{1}{2} I_{f2} N \Lambda_0 [\cos(2\omega t + \alpha_m) + \cos(2\omega t - \alpha_m)] \cdot \\ \quad \cos(\omega t - \alpha_m + 0.5\pi + \varphi) + \eta I_{f0} N \Lambda_0 \cos(\omega t - \alpha_m) \\ \quad - \frac{1}{2} \eta I_{f2} N \Lambda_0 \cos(2\omega t + \alpha_m) \cdot \\ \quad [\cos(\omega t + \alpha_m) + \cos(3\omega t - \alpha_m)] - \frac{1}{2} \eta I_{f2} N \Lambda_0 \cos(2\omega t - \alpha_m) \cdot \\ \quad [\cos(\omega t + \alpha_m) + \cos(3\omega t - \alpha_m)] \quad \dots \dots \text{SISC} \end{array} \right. \quad (8)$$

where  $\eta$  is the coefficient of the stator MMF to the rotor MMF. It is important to note that  $2\omega$  is the frequency of the reverse electromotive force induced by the excitation windings under the SISC condition.

As indicated in (8), only the first harmonic exists in the ideally normal condition, while the extra third and fifth harmonics are induced under the SISC condition. Meanwhile, the harmonic amplitudes are decreased as the SISC degree, which is represented by  $I_{f2}$ , intensifies.

Besides, observing (4) and (8), only the fundamental harmonic of the MMF is illustrated. However, other odd harmonics also exist under the actual condition. Since the other harmonics are very similar to the fundamental harmonic and the space is limited, the analysis is not listed individually.

## 2.2 | Shaft voltage model

Generally, the shaft voltage refers to the potential difference between the two ends of the rotating shaft of the generator [24]. The fluxes per pole in generators can be divided into two equal fluxes, namely, the clockwise flux and the anticlockwise flux. Normally, the clockwise flux is equal to the anticlockwise flux. However, the net dissymmetry flux is yielded due to the dissymmetry MFD as the SISC takes place. When the generator rotates, the magnetic flux links with the shaft and the shaft voltage is induced, as shown in Figure 2.

In order to clearly calculate the shaft voltage, the MFD is divided into five parts under the SISC condition. Particularly,  $B_3$  and  $B_4$  are generated by the excitation windings, while  $B_5$ ,  $B_6$  and  $B_7$  are generated by the armature windings.

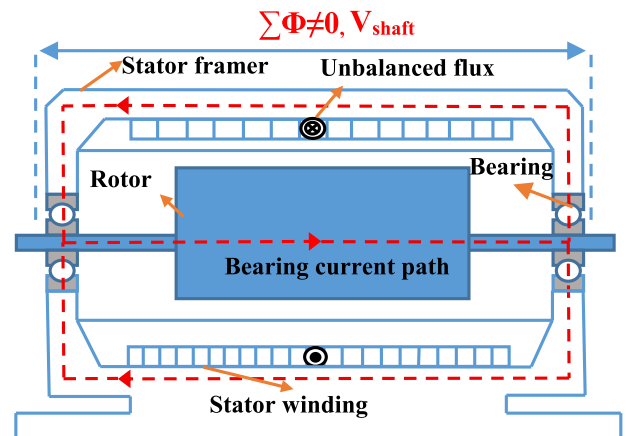


FIGURE 2 Schematic diagram of shaft voltage.

$$\left\{ \begin{array}{l} B_3 = I_{f_0} N \Lambda_0 \cos(\omega t - \alpha_m + 0.5\pi + \varphi) \\ B_4 = -\frac{1}{2} I_{f_2} N \Lambda_0 [\cos(2\omega t + \alpha_m) \\ \quad + \cos(2\omega t - \alpha_m)] \cdot \cos(\omega t - \alpha_m + 0.5\pi + \varphi) \\ B_5 = \eta I_{f_0} N \Lambda_0 \cos(\omega t - \alpha_m) \\ B_6 = -\frac{1}{4} \eta I_{f_2} N \Lambda_0 [\cos(3\omega t + 2\alpha_m) + \cos \omega t \\ \quad + \cos 5\omega t + \cos(\omega t - 2\alpha_m)] \\ B_7 = -\frac{1}{4} \eta I_{f_2} N \Lambda_0 [\cos 3\omega t + \cos(\omega t - 2\alpha_m) \\ \quad + \cos(5\omega t - 2\alpha_m) + \cos \omega t] \end{array} \right. \quad (9)$$

According to Faraday's law of electromagnetic induction, the expression of shaft voltage is as follows:

$$V_{shaft} = \frac{\partial \left( \int_0^{2\pi} B(\alpha_m, t) d\alpha_m \right) S}{\partial t} \quad (10)$$

Ultimately, the shaft voltage under the normal SISC conditions can be expressed as follows:

$$\left\{ \begin{array}{l} V_1 = 0 \quad \dots \dots \text{Normal} \\ V_2 = \frac{1}{2} \pi I_{f_2} N \Lambda_0 [3\omega \sin(3\omega t + 0.5\pi + \varphi) \\ \quad + \omega \sin(\omega t - 0.5\pi - \varphi)] S + \frac{1}{2} \pi \eta I_{f_2} N \Lambda_0 [2\omega \sin \omega t \\ \quad + 3\omega \sin 3\omega t + 5\omega \sin 5\omega t] S \quad \dots \dots \text{SISC} \end{array} \right. \quad (11)$$

As indicated in (11), there is no shaft voltage under the normal condition, while under the SISC condition, the shaft voltage is produced, with first, third and fifth harmonics.

### 3 | FEA AND EXPERIMENTAL VALIDATION

#### 3.1 | FEA and experimental setup

The focus of the work is to monitor changes of the shaft voltage as the SISC intensifies. Thus, a 5 kW prototype synchronous generator (2-pole/36-slot) is designed and manufactured to verify the proposed theoretical model. The prototype can simulate different SISC degrees by changing the number of the short-circuit turns. The prototype is applied in

the experiments and the rated rotating speed is 3000 rpm in order to ensure the electrical frequency. Meanwhile, the EFA model of the corresponding entity is established with fidelity. Besides, the full load is taken into consideration in both the FEA calculation and the experiments. The main parameters of the generator are shown in Table 1.

During the FEA calculation, the overall setup can be divided into the physical model part and the external coupling circuit part, as illustrated in Figure 3a, b, respectively. The FEA model is illustrated in Figure 3a. The SISC fault is simulated by modifying both the external coupling circuit (see Figure 3b) and the physical model (the failure windings are divided into two parts: one is to simulate the healthy part while the other is to simulate the short circuit part, see Figure 3a). The different degree of the SISC is simulated by adjusting the turn numbers of PA1\_short (the short circuit part) and PA1 (the healthy part), as indicated in Figure 3b.

In order to obtain the shaft voltage signal during the simulation calculation, the shaft is equivalent to a single turn winding approximately. The rotation of the shaft does not affect the shaft voltage signal. In the simulation iteration, the shaft voltage is generated in the equivalent winding. The issue that needs specific attention is the equivalent winding, which does not appear in the coupling circuit. In fact, the equivalent winding is an open circuit because only the voltage signal is required and the current signal is not required. And no external incentive is needed in the equivalent winding. Besides, the coupling circuit only consists of the stator winding coupling circuit and the field winding coupling circuit.

During the experiment, the shaft voltage is measured using a special device designed and manufactured by the authors based on the definition of the shaft voltage. The device is composed of a carbon brush to test the voltage potential on the driven end and a transmission line to test the voltage potential on the non-driven end, as illustrated in Figure 4a. And the measurement scheme of the shaft voltage is shown in Figure 4b. Further, the carbon brush and the transmission line are connected to the signal collector. The data of the shaft voltage sign can be acquired using the signal collector.

Particularly, there is a plate with several short circuit taps of phase A on the prototype. Each short-circuit degree corresponds to several short-circuit turns, respectively. Different

TABLE 1 Primary parameters of the prototype generator

Parameters	Values	Parameters	Values
Rated power	5 kVA	Outer diameter of the stator	250.5 mm
Rated voltage	380 V	Inner diameter of the stator	145 mm
Rated rotating speed	3000 rpm	Stator core length	130 mm
Rated power factor	0.8	Outer diameter of the rotor	142.6 mm
Radial air-gap length	1.2 mm	Pole-pairs	1
Stator slots	36	Parallel branches	2

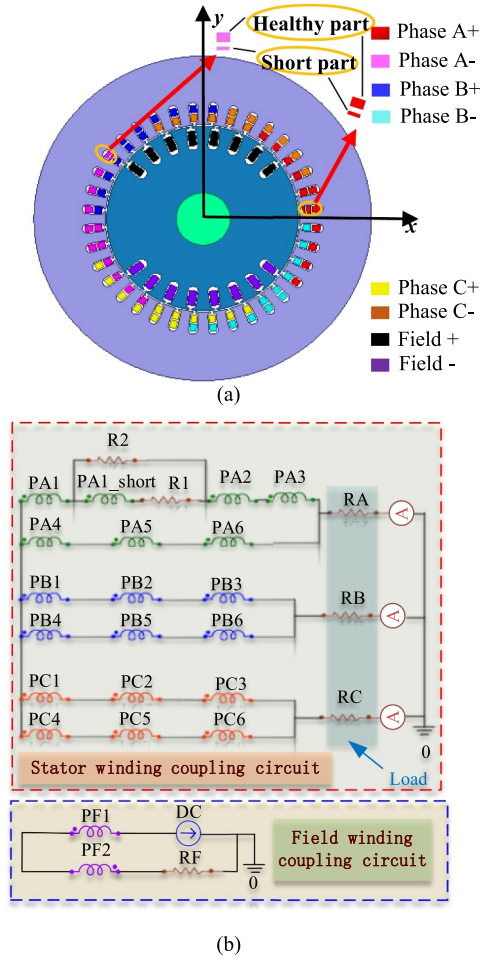


**FIGURE 3** CS-5 finite element simulation setup: (a) physical 2D model and (b) coupling circuit model.

stator short-circuit degrees are simulated by connecting different short-circuit taps to realise shorting different number of the stator winding turns, see Figure 4a. Two groups of the FEA calculation and the experiments are respectively taken as follows:

- (1) Normal condition. There is no SISC with full load.
- (2) SISC conditions. 3%, 6%, and 9% SISC conditions are taken with full load, respectively.

## 3.2 | Results and discussion

### 3.2.1 | MFD result

The air-gap MFD results by the FEA calculation at 0.06s are illustrated in Figure 5. It is shown that the MFD amplitude is decreased as the SISC takes place. The increment of the SISC degree decreases the MFD amplitude. The result is consistent with the conclusion from (8).

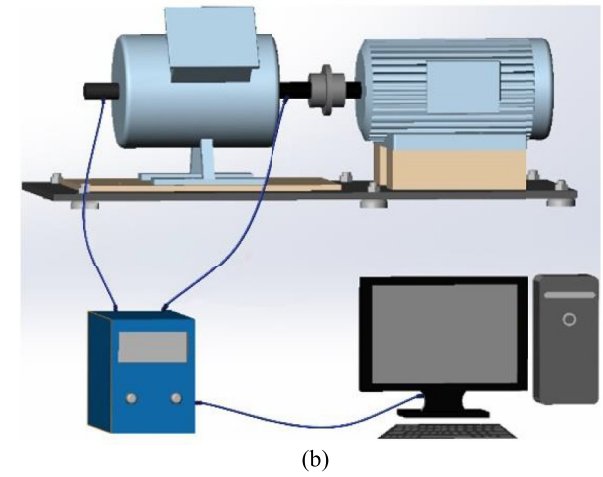
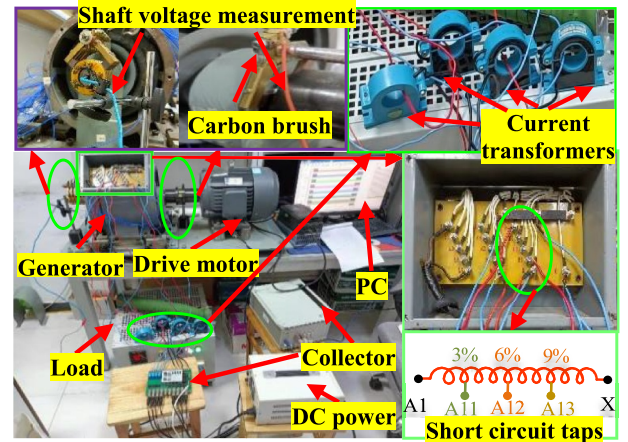


**FIGURE 4** CS-5 experimental setup: (a) experimental model and (b) process simplification model.

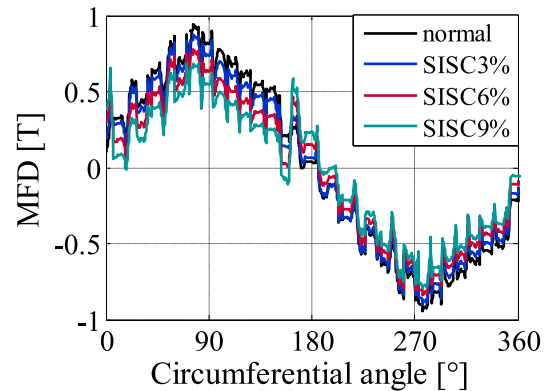


**FIGURE 5** Magnetic flux density (MFD) results by finite element analysis (FEA).

The three-phase current results by the simulating calculation are illustrated in Figure 6. It is clearly shown that the amplitudes of the three-phase current are the same under the

normal condition in Figure 6a. Obviously, the clockwise and anticlockwise magnetic fluxes are equal in the magnetic circuit of synchronous generators. As shown in Figure 6b–d, the three-phase current is asymmetrically distributed in the space due to the ring current in the short-circuited ring under the SISC conditions. Further, the difference between the three phase currents becomes more obvious with the increase of the short-circuit degree. A special note is needed that the short circuit occurs in phase A, and phase B is closer to the position of the short circuit than phase C in Figure 3a. Hence, the unbalanced current will produce the asymmetrical magnetic flux under SISC conditions.

Further, this difference creates the magnetic linkage around the shaft as the shaft rotates. The shaft voltage is induced based on the law of electromagnetic induction. In order to analyse the generation of shaft voltage and asymmetrical magnetic flux in detail, the detailed magnetic flux lines (MFL) distribution in the generator is indicated in Figure 7. It is clear that the distribution is symmetric under the normal condition, as shown in Figure 7a. As SISC takes place, the distribution changes from symmetric to asymmetric, leading to the generation of the shaft voltage. It is suggested from Figure 7b–d that the asymmetry trend will be increased as the short circuit degree increases.

For a further representation, the maximum values of the MFL in different directions are displayed in Figure 8. At this time, the positive MFL can be regarded as a clockwise direction and the negative MFL as a counterclockwise direction; then the

asymmetrical magnetic flux can be expressed according to the changes of their peaks. It is clear that the maximum value of MFL in the clockwise direction is 5.50, 4.99, 4.31 and 3.86, respectively, yet the maximum value of MFL in the anticlockwise direction is 5.50, 5.11, 4.65 and 4.29, respectively. Hence, the asymmetrical magnetic flux will be clearly enlarged as the short-circuit degree increases.

### 3.2.2 | Shaft voltage result

The shaft voltage results obtained using the FEA calculation and experiments are illustrated in Figures 9 and 10, respectively. Theoretically, the shaft voltage should be zero under the normal condition in Figures 9a and 10a. However, the inaccurate assembling and the manufacturing errors will break the MFD distribution balance and have an obvious impact on the shaft voltage. As the SISC takes place, the MFD distribution balance is further damaged, and consequently, the shaft voltage is also increased, especially as the short circuit degree increases.

In Figures 9b and 10b, it is clear that the occurrence of the SISC brings in the shaft voltage composed of first, third, and fifth harmonics. Moreover, as the SISC degree increases, the amplitudes of first, third, and fifth harmonics will all be increased. This is consistent with the qualitative conclusion based on (11).

The FEA and the experimental results are compared in Figure 11. It is shown that although the amplitude

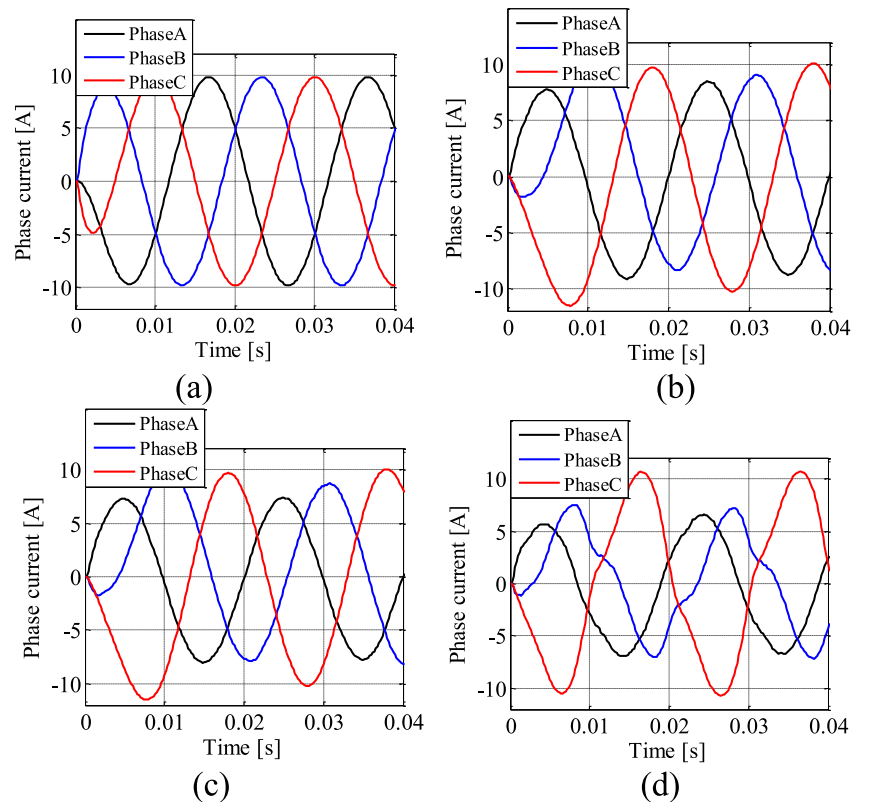


**FIGURE 6** Phase current: (a) normal, (b) stator interturn short circuit (SISC) 3%, (c) SISC 6% and (d) SISC 9%.

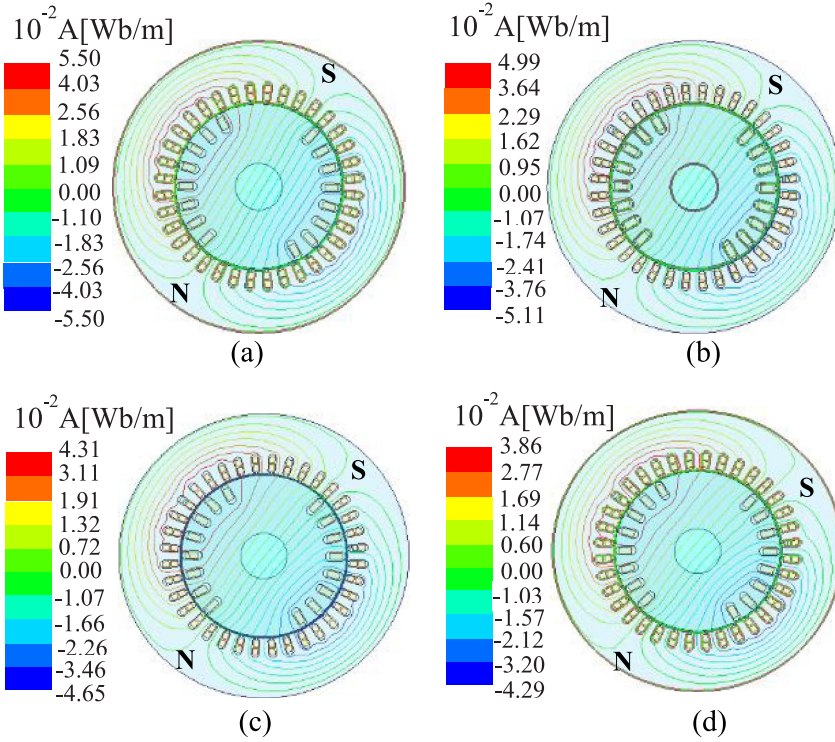


**FIGURE 7** Magnetic flux lines (MFL) distribution: (a) normal, (b) stator interturn short circuit (SISC) 3%, (c) SISC 6% and (d) SISC 9%.

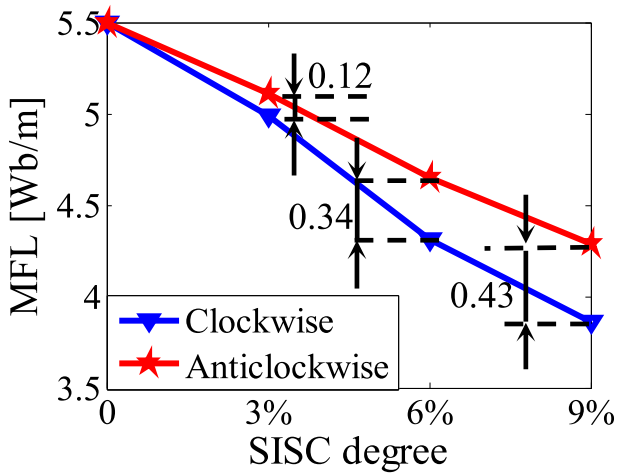


**FIGURE 8** Maximum magnetic flux lines (MFL) in a different stator interturn short circuit (SISC) fault degree.

increment of FEA is not exactly equal to the experimental result, the developing tendencies are generally consistent with each other. Besides, both the FEA results and the experiment data match the previous theoretical analysis conclusion.

The issue that needs special attention is the amplitude of the first harmonic in Figure 11a. The significant difference of the first harmonic is mainly caused by the stator and rotor vibration. In Refs. [25, 26], compared with the normal condition, the vibration of the stator and the rotor intensifies under the SISC condition. And the vibration increases obviously as the SISC intensifies. Compared with the other case, the

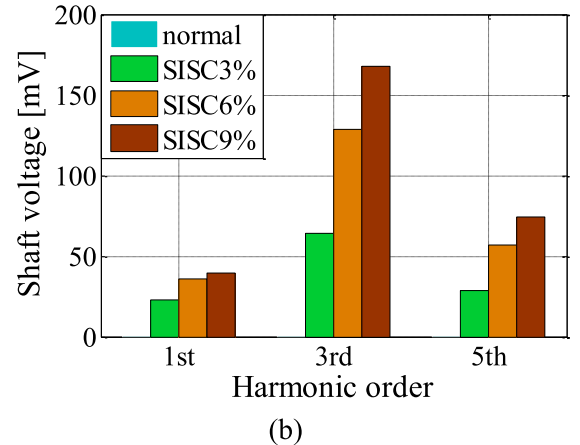
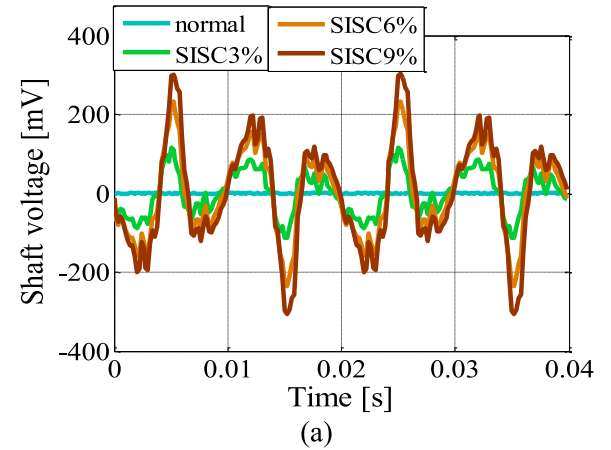
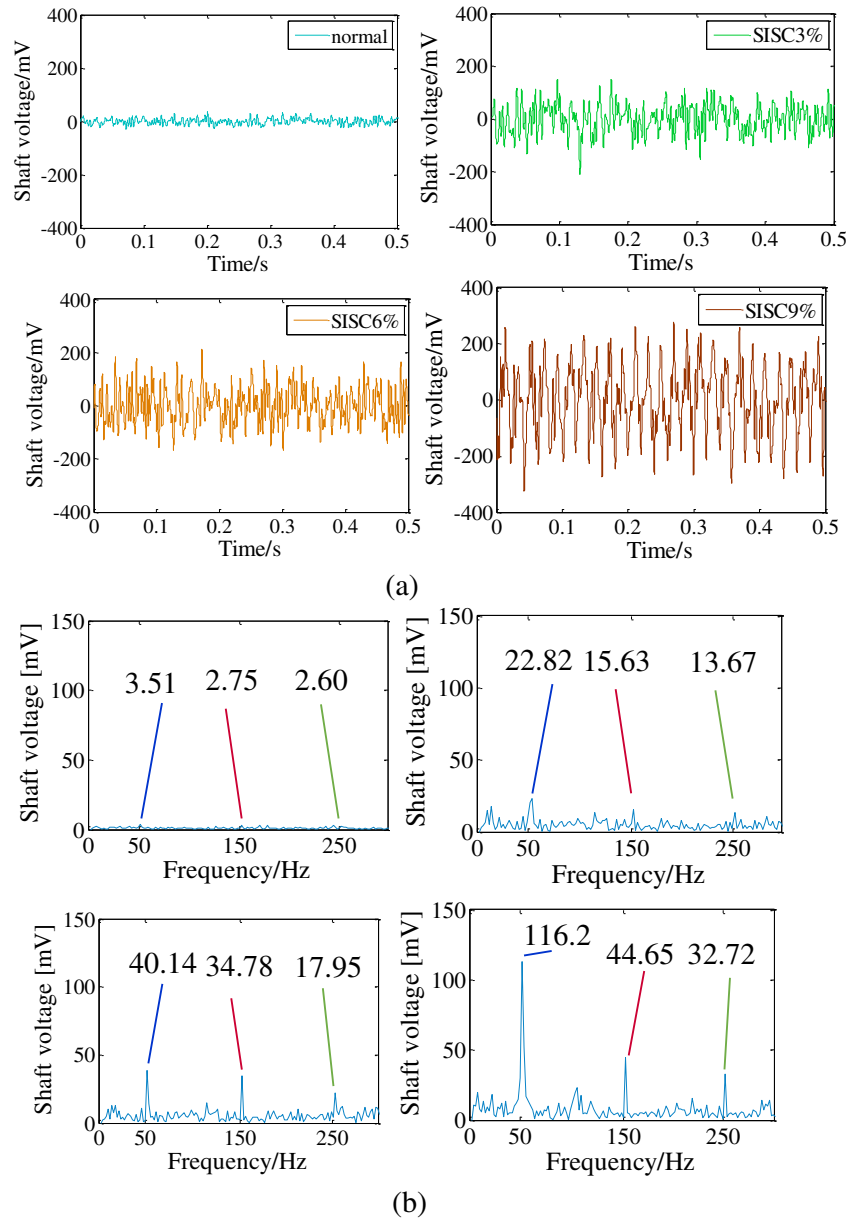


**FIGURE 9** Finite element analysis (FEA) data of shaft voltage under the stator interturn short circuit (SISC) fault: (a) time domain waveform and (b) harmonic order in different SISC degrees.

**FIGURE 10** Experimental data of shaft voltage under the stator interturn short circuit (SISC) fault: (a) time domain waveform: normal, 3%, 6%, and 9% SISC condition and (b) frequency domain waveform: normal, 3%, 6%, and 9% SISC condition.



vibration amplitude in the SISC 9% case is larger. Further, the excessive vibration inevitably leads to the occurrence of the eccentricity. Meanwhile, it is worth noting that shaft voltage is mainly composed of the first harmonic under the eccentric fault [15]. Hence, the first harmonic amplitude variation of the shaft voltage obtained using the experiment is higher than that obtained using the FEA calculation.

## 4 | CONCLUSION

In this paper, the characteristics of the shaft voltage under the SISC condition are comprehensively analysed. Theoretical analysis, FEA calculation, and experimental studies are carried out together to obtain the impact of SISC on the characteristics

of the shaft voltage. The key conclusions drawn from the study are as follows:

- (1) The detailed expressions of the shaft voltage under both the normal and SISC conditions are derived based on the magnetic flux density variation. It is shown that in SISC cases, the shaft voltage composed of first, third, and fifth harmonics is induced in synchronous generators.
- (2) A specific device to test the shaft voltage is designed and manufactured by the authors. By employing the device, the experiments are carried out to obtain the shaft voltage signals, and the experimental results show that the shaft voltage is very tiny under the normal condition due to the manufacturing and assembling errors. The occurrence of SISC considerably enlarges the shaft voltage.

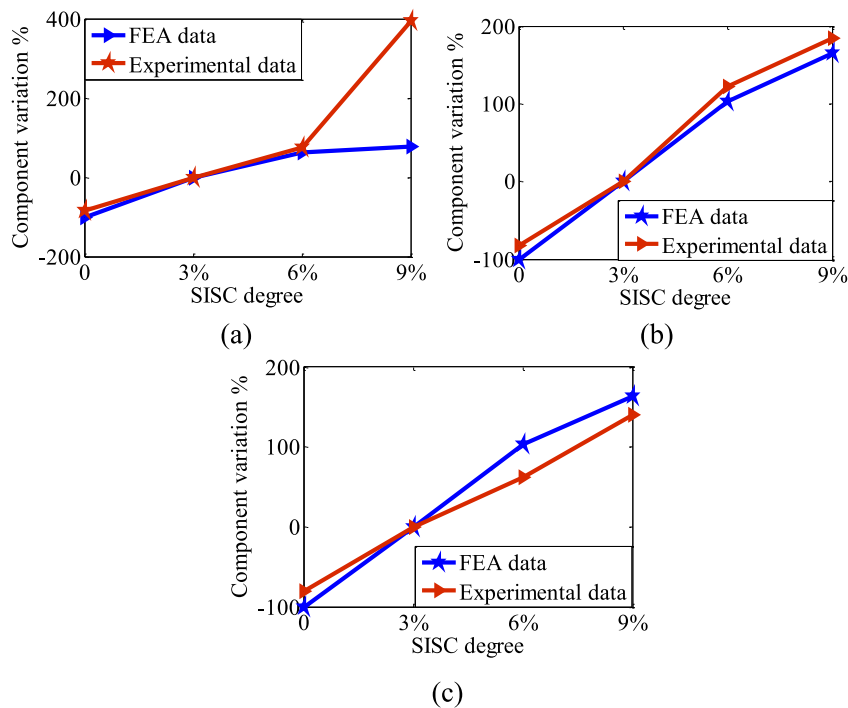


**FIGURE 11** Finite element analysis (FEA) and experiment comparison in stator interturn short circuit (SISC) cases: (a) first harmonic, (b) third harmonic, and (c) fifth harmonic.

The study conclusions as well as the specific shaft voltage testing device designed by the authors provide an important supplement to the current knowledge base and have high potential to be applied for SISC fault detection and diagnosis in synchronous generators.

### AUTHOR CONTRIBUTIONS

Conceptualisation: Yu-Ling He, Pei-Jie Yang and Kai Sun. Methodology: Yu-Ling He, Pei-Jie Yang and Kai Sun. Software: Yu-Ling He, Pei-Jie Yang, Kai Sun, Zhen-li Xu. Validation: Pei-Jie Yang, Kai Sun, Hai-peng Wang. Formal analysis: Yu-Ling He. Investigation: Yu-Ling He, Pei-Jie Yang. Resources: Yu-Ling He, Hai-peng Wang. Data curation: Yu-Ling He, Pei-Jie Yang, Xian-Long He. Writing—original draft preparation: Yu-Ling He, Pei-Jie Yang, Kai Sun, Zhen-li Xu, Hai-peng Wang, Xian-Long He. Writing—review and editing: Yu-Ling He, Pei-Jie Yang, Kai Sun, David Gerada. Supervision: Yu-Ling He, David Gerada. Project administration: Yu-Ling He, Pei-Jie Yang and Kai Sun. Funding acquisition: Yu-Ling He, Xian-Long He. All authors have read and agreed to the published version of the manuscript.

### ACKNOWLEDGEMENTS

This work was supported in part by the National Natural Science Foundation of China (52177042), the Hebei Provincial Natural Science Foundation (E2020502031), the Chinese Fundamental Research Funds for the Central Universities (2020MS114 and 2018YQ03), Suzhou Social Developing Innovation Project of Science and Technology (SS202134), and the third Top Youth Talent Support Program of Hebei Province ([2018]-27).

### CONFLICT OF INTEREST

There are no conflicts of interest.

### DATA AVAILABILITY STATEMENT

Data sharing not applicable to this article as no data sets were generated or analysed during the current study.

### ORCID

Yu-Ling He  <https://orcid.org/0000-0003-2719-8128>

Hai-Peng Wang  <https://orcid.org/0000-0003-4612-2874>

### REFERENCES

- Plazenet, T., et al.: A comprehensive study on shaft voltages and bearing currents in rotating machines. *IEEE Trans. Ind. Appl.* 54(4), 3749–3759 (2018). <https://doi.org/10.1109/tia.2018.2818663>
- Hoffe, S.J., Meyer, A.S., Cronje, W.A.: Determination of shaft position from shaft voltage on a synchronous generator. In: 2005 5th IEEE International Symposium on Diagnostics for Electric Machines, Power Electronics and Drives, pp. 1–4. (2005)
- Berhausen, S., Jarek, T.: Method of limiting shaft voltages in AC electric machines. *Energies* 14(11), 1–19 (2021). <https://doi.org/10.3390/en14113326>
- Punga, F., Hess, W.: Bearing currents. *Elektrotech Maschinenbau* 25(8), 615–618 (1907)
- Alger, P., Samson, H.: Shaft currents in electric machines. *Trans. AIEE* 43(5), 235–238 (1924). <https://doi.org/10.1109/jaiee.1924.6537807>
- Doorsamy, W., et al.: An experimental design for static eccentricity detection in synchronous machines using a Cramér–Rao lower bound technique. *IEEE Trans. Energy Convers.* 30(1), 254–261 (2015). <https://doi.org/10.1109/tec.2014.2347895>
- Peng, B., Wang, X., Zhao, W.: Research on shaft voltage in permanent magnet synchronous machine with sectionalized stators. In: 2017 20th International Conference on Electrical Machines and Systems (ICEMS), pp. 1–5. (2017)

8. Datta, A.K., Dubey, M., Jain, S.: Effect of static power supply in alternator used for short-circuit testing-observation of shaft voltage. *IEEE Trans. Power Electron.* 29(11), 6074–6080 (2014). <https://doi.org/10.1109/tpel.2014.2300185>
9. Peng, B., Zhao, W., Wang, X.: The method for reducing intrinsic shaft voltage by suitable selection of pole-arc coefficient in fractional-slot permanent-magnet synchronous machines. *IEEE Trans. Magn.* 54(11), 1–5 (2018). <https://doi.org/10.1109/tmag.2018.2834536>
10. Chen, L., et al.: A survey on shaft voltage of large generator. In: *Applied Mechanics & Materials*, pp. 1445–1448. (2014)
11. Golkhandan, R.K., Torkaman, H.: Reduction of induced shaft voltage and bearing current in turbo generators: modeling, compensation, and practical test. *IEEE Trans. Ind. Electron.* 68(5), 4362–4372 (2021). <https://doi.org/10.1109/tie.2020.2985006>
12. Park, J.K., et al.: Mitigation method of the shaft voltage according to parasitic capacitance of the PMSM. *IEEE Trans. Ind. Appl.* 53(5), 4441–4449 (2017). <https://doi.org/10.1109/tia.2017.2717378>
13. He, Y.-L., et al.: A novel universal model considering SAGE for MFD-based faulty property analysis under RISC in synchronous generators. *IEEE Trans. Ind. Electron.* 69(7), 7415–7427 (2022). <https://doi.org/10.1109/tie.2021.3094481>
14. Nippes, P.I.: Early warning of developing problems in rotating machinery as provided by monitoring shaft voltages and grounding currents. *IEEE Trans. Energy Convers.* 19(2), 340–346 (2004). <https://doi.org/10.1109/tec.2004.827471>
15. Wu, Y.-C., et al.: Diagnosis of non-salient pole synchronous generator rotor's typical faults based on shaft voltage. *Trans. Electrotech. Soc.* 25(6), 178–184 (2010)
16. Li, H.-M., et al.: Influence of rotor windings inter-turn short circuit fault on electric machine shaft voltage. *Proc. CSEE* 29(36), 96–100 (2009)
17. Darques, K., et al.: Effect of end windings on the shaft voltage of a high power alternator using FE analysis. *Int. J. Appl. Electromagn. Mech.* 63(2), 1–11 (2020). <https://doi.org/10.3233/jae-209202>
18. Grubic, S., et al.: A survey on testing and monitoring methods for stator insulation systems of low-voltage induction machines focusing on turn insulation problems. *IEEE Trans. Ind. Electron.* 55(12), 4127–4136 (2008). <https://doi.org/10.1109/tie.2008.2004665>
19. Obeid, N.H., Boileau, T., Nahid-Mobarakeh, B.: Modeling and diagnostic of incipient interturn faults for a three-phase permanent magnet synchronous motor. *IEEE Trans. Ind. Appl.* 52(5), 4426–4434 (2016). <https://doi.org/10.1109/tia.2016.2581760>
20. Bouzid, M.B.K., et al.: An effective neural approach for the automatic location of stator interturn faults in induction motor. *IEEE Trans. Ind. Electron.* 55(12), 4277–4289 (2008). <https://doi.org/10.1109/tie.2008.2004667>
21. Sarikhani, A., Mohammed, O.A.: Inter-turn fault detection in PM synchronous machines by physics-based back electromotive force estimation. *IEEE Trans. Ind. Electron.* 60(8), 3472–3484 (2013). <https://doi.org/10.1109/tie.2012.2222857>
22. He, Y.-L., et al.: A new external search coil based method to detect detailed static air-gap eccentricity position in nonsalient pole synchronous generators. *IEEE Trans. Ind. Electron.* 68(8), 7535–7544 (2021). <https://doi.org/10.1109/tie.2020.3003635>
23. He, Y.-L., et al.: Effect of static eccentricity and stator inter-turn short circuit composite fault on rotor vibration characteristics of generator. *Trans. Can. Soc. Mech. Eng.* 39(4), 767–781 (2015). <https://doi.org/10.1139/tcsme-2015-0061>
24. Otto, H.: Influence of shaft voltage and bearing current and their causes on motor and remedial measures. *Motor Transl.* 61, 14–27 (1996)
25. Ma, J., et al.: Structural optimization of a permanent-magnet direct-drive generator considering eccentric electromagnetic force. *IEEE Trans. Magn.* 51(3), 1–4 (2015). <https://doi.org/10.1109/tmag.2014.2361871>
26. He, Y.-L., et al.: Impact of stator interturn short circuit position on end winding vibration in synchronous generators. *IEEE Trans. Energy Convers.* 36(2), 713–724 (2021). <https://doi.org/10.1109/tec.2020.3021901>

**How to cite this article:** He, Y.-L., et al.: Impact of stator interturn short circuit fault on shaft voltage in synchronous generator. *IET Electr. Power Appl.* 1–11 (2022). <https://doi.org/10.1049/elp2.12271>